OPEN ACCESS

Impact of GDC Interlayer Microstructure on Strontium Zirconate Interphase Formation and Cell Performance

Journal of The Electrochemical Society, 2023 **170** 104501

Impact of GDC Interlayer Microstructure on Strontium Zirconate Interphase Formation and Cell Performance

Sadhana Golani,[1,z] Florian Wankmüller,[2] Werner Herzhof,[3] Christian Dellen,[3] Norbert H. Menzler,[3] and André Weber[1]

[1]*Institute for Applied Materials - Electrochemical Technologies (IAM-ET), Karlsruhe Institute of Technology (KIT), D-76131 Karlsruhe, Germany*
[2]*Laboratory for Electron Microscopy (LEM), Karlsruhe Institute of Technology (KIT), D-76131 Karlsruhe, Germany*
[3]*Forschungszentrum Jülich GmbH, Institute of Energy and Climate Research (IEK), IEK-1: Materials Synthesis and Processing D-52425 Jülich, Germany*

In solid oxide cells (SOCs) exhibiting mixed ionic-electronic conductor air electrode (MIEC AE) (e.g. $La_{0.6}Sr_{0.4}Co_{0.2}Fe_{0.8}O_{3-\delta}$ LSC(F)), the formation of insulating zirconate interphases at the air electrode/zirconia electrolyte—interface is commonly prevented by an interlayer of doped cerium oxide. This complex interaction has a tremendous influence on cell performance, as the morphology of the interlayer determines the amount and continuity of the zirconate interphases. The performance of fuel electrode supported cells (FESCs) exhibiting gadolinium-doped ceria (GDC) interlayers fabricated from different commercially available powders are compared. All of these layers were fabricated according to the same procedure. The cell performance is analyzed by means of current-voltage (CV) characteristics, electrochemical impedance spectroscopy (EIS) and subsequent impedance analysis by the distribution of relaxation times (DRT). Next to the cell testing at application-oriented conditions, impedance spectra are measured over a wide temperature ranging down to 250 °C to resolve polarization phenomena related to bulk, grain boundary and interfacial effects within and in-between the gadolinium-doped ceria (GDC) and the 8 mol% yttria-stabilized zirconia (8YSZ) electrolyte. Furthermore, symmetrical air electrode (SymAE) cells are analyzed to eliminate impedance contributions from the anode layer (AL) and the substrate. The electrochemical results are correlated to the microstructural features of the GDC/YSZ interface obtained from post-test focused ion beam (FIB)/scanning electron microscope (SEM) analysis. This comparison revealed significant differences in the cell performance, which could be attributed to the amount and continuity of the residual strontium zirconate (SZO) interphase.

 [DOI: 10.1149/1945-7111/acfc2c]

Manuscript submitted February 20, 2023; revised manuscript received August 24, 2023. Published October 4, 2023.

List of Symbols

Abbreviations

AC	Alternating Current
AE	Air Electrode
AL	Anode layer
BET	Brunauer–Emmett–Teller
CV	Current-Voltage
DC	Direct Current
DRT	Distribution of Relaxation Times
EIS	Electrochemical Impedance Spectroscopy
ESC	Electrolyte Supported Cells
FESCs	Fuel Electrode Supported Cells
FIB	Focused Ion Beam
GDC	10 mol% Gd_2O_3 doped CeO_2 (Gadolinium-Doped Ceria)
H_2	Hydrogen
H_2O	Steam
ICD	In-Column Detector
ID	Interdiffusion
LSCF	$La_{0.6}Sr_{0.4}Co_{0.2}Fe_{0.8}O_{3-\delta}$
MIEC	Mixed Ionic-Electronic Conductor
MFC	Mass Flow Controllers
MD	Mirror Detector
OCV	Open-Circuit-Voltage
PLD	Pulsed Layer Deposition
PVD	Physical Vapor Deposition
SOC	Solid Oxide Cells
SEM	Scanning Electron Microscope
SOP	Standard Operation Procedures
SymAE	Symmetrical Air Electrode
SZO	Strontium Zirconate
TLM	Transmission Line Model
8YSZ	8 mol% yttria-stabilized zirconia

Solid Oxide Cells (SOCs) designated for low (below 600 °C) and intermediate (800 °C–600 °C) operating temperatures require a highly efficient air electrode.[1,2] $La_{1-x}Sr_xCo_{1-y}Fe_yO_3$ (LSCF), a Mixed Ionic-Electronic Conductor (MIEC), enables fast oxygen-exchange kinetics and is nowadays preferentially utilized for the air electrode in high performance cells targeting an operating temperature range from 850 °C to 600 °C.[2] The major drawback of LSCF is its instability against Zr-based electrolytes. At the LSCF/doped zirconia interface, strontium and zirconium react and a Strontium Zirconate $SrZrO_3$ (SZO) -phase is formed.[1,2] This interphase acts as an oxygen ion blocking layer and degrades the cell performance and its formation is unavoidable during sintering at elevated temperatures.[3]

In order to suppress this secondary phase formation, a spatial separation of LSCF and YSZ is realized by the insertion of a doped ceria interlayer.[3] Nowadays the most common material for this interlayer is Gd-doped CeO_2 (GDC). This layer should be dense to prevent Sr-transport via surface diffusion along the GDC surfaces as well as gas diffusion via $Sr(OH)_2$ in connected tubular-shaped pores.[4] On the other hand, the high sintering temperatures required to densify screen-printed printed GDC layers are accompanied by an interdiffusion at the GDC/YSZ interface, resulting in an interdiffusion zone about one order of magnitude of lower conductivity.[2,5]

Furthermore, the sintering shrinkage of the GDC layer comes along with extended mechanical stress resulting in warpage of the cell. After manufacturing a flat half-cell, consisting of support/fuel electrode/electrolyte, by tape casting, screen printing and subsequent sintering and ironing steps, the GDC layer is screen printed and sintered at 1300 °C. Sintering at significantly higher temperatures resulted in an irreversible bending of the cell that could not be removed by additional ironing steps. Furthermore, the solid state

[z]E-mail: sadhana.golani@kit.edu

interdiffusion at the YSZ/GDC interface is enhanced. These issues could be resolved by alternative processing routes such as sputtering, Physical Vapor Deposition (PVD)[3] or Pulsed Laser Deposition (PLD),[6] which are avoided in commercial products as they are time consuming and costly. In the case of screen printed and sintered GDC-interlayers a compromise regarding the sintering temperature is found. In this case, SZO-formation is not fully prevented but solid state interdiffusion between GDC and YSZ as well as resistance can be limited to an acceptable level.[1,7] The influence of the GDC interlayer sintering temperature on the morphology of SZO formed in the subsequent sintering step of the LSCF-cathode was reported in previous studies.[1,3,8] A continuous SZO interphase in between GDC and YSZ, which was formed for GDC interlayers sintered at low temperatures (1100 °C), resulted in a severely altered polarization resistance.[2] With increasing sintering temperature, the resistance decreased by several orders of magnitude, which could be attributed to an increasing number of conductive gaps in the SZO-interphase. It could be shown that not the total amount of SZO but the missing continuity of the SZO-interphase was leading to the performance improvement. At much higher sintering temperatures (1400 °C) almost no SZO was formed.[2]

Regarding the industrialization of SOC technology, the secured availability of commercial raw materials is of utmost importance. Considering the supply of powders, the delivery capability of a single supplier might be temporarily limited and second sources should be available. Powders from second sources should ideally exhibit not only a similar composition but also similar morphology and impurity contents, as all of these parameters can affect sintering behavior, resulting in microstructure and even secondary phase formation.

To illustrate such correlations, in this study the performance of cells with identically manufactured GDC-interlayers produced from three different commercially available GDC ($Ce_{0.8}Gd_{0.2}O_{2-\delta}$) powders is compared. Powders with rather similar morphological properties were selected to enable similar processing and therefore avoid the need to develop an adapted processing route for each powder.

The performance was evaluated in full and symmetrical cells applying Direct Current (DC) and Alternating Current (AC) methods. Post-test analysis was performed by means of Focused Ion Beam (FIB) and Scanning Electron Microscope (SEM). Despite the similar material composition and processing route, the remaining differences in the powders resulted in microstructural differences affecting SZO distribution at the GDC/YSZ interface and thus cell performance.

Experimental

Two different types of cells were investigated in this study, (i) Fuel-Electrode Supported Cells (FESC) exhibiting a Ni/8YSZ substrate and fuel electrode, an 8YSZ-electrolyte, the GDC-interlayer and an LSCF air electrode ($La_{0.58}Sr_{0.4}Co_{0.2}Fe_{0.8}O_{3-\delta}$) and (ii) electrolyte-supported Symmetrical Air Electrode cells (SymAE) based on an 8YSZ-substrate coated with the GDC-interlayer and an LSCF air electrode on both sides. The production of the FESCs is described in Refs. 7, 9 in detail, but is briefly summarized here: the support is tape cast and pre-sintered. All functional layers, the electrodes, the electrolyte and the barrier layer are screen printed and sequentially sintered at the appropriate temperatures. Every half-cell consisting of the support, the electrode and the electrolyte is tested with respect to gas tightness by a window leak test prior to barrier layer and air-electrode deposition. The internal threshold value for air gas tightness is 5.8×10^{-6} h Pa dm^3 s^{-1} cm^{-2} and all the samples tested here, fulfill that criterion. The half-cells were provided by the company Ceramtec (Ceramtec AG, Marktredwitz, Germany) in order to keep them similar as much as possible. Only the varied GDC barrier layer and the air electrode were applied internally according to our internal specifications and the Standard Operation Procedures (SOP).

In the case of the symmetrical cells, GDC-interlayers and LSCF-electrodes were applied to a commercially available 8YSZ-susbtrate from Kerafol (Kerafol GmbH, Eschenbach in der Oberpfalz, Germany). For the manufacturing of the GDC-interlayers, powder conditioning, paste preparation, screen printing and subsequent sintering at 1300 °C were performed identically using a well-defined processing route.[7] The only difference in the preparation process of the GDC-interlayers was the three different commercially available GDC-powders GDC 1, GDC 2 and GDC 3 from three different companies.

The processing was intentionally not adapted to the powder morphologies of the three powders to enhance the visibility/comprehensibility of the powder properties—microstructure/foreign phase formation—performance interaction. As stated in Szasz et al.,[2] the major part of minimizing the interaction of Sr from the air electrode with the YSZ electrolyte is the existence of the interdiffusion layer between YSZ and GDC. It does not drastically depend on the density of the GDC layer hence their function as diffusion barrier layers might also not differ significantly. If a "good" interdiffusion layer is formed, less SZO is formed. Thus, the necessity of making the GDC diffusion barrier layer dense is not accustomed and the powders can be directly used as provided by the companies.

GDC powder characteristics.—Three different commercially available GDC powders were used: GDC 1: Treibacher Industrie AG (usually used powder; Althofen, Austria), GDC 2: Solvay Special Chemicals (Anan City, Japan) and GDC 3: KCeracell (Geumsan-gun, South Korea). Andreas et al. had used a similar powder commercially produced by the Treibacher Industrie at that time. The results concluded that the grain size as well as the sintering temperature affected the electrochemical performance. Furthermore, the fine powder with a mean particle size of d50 = 0.2 μm and reduced with the same well-defined reduction procedure resulted in the best performance.[10] However, in recent times Treibacher Industrie AG has been supplying the fine powder with a mean particle size of d50 = 0.29 μm as mentioned in Table I (named as GDC1). Therefore, GDC 1 is used as a reference and compared with the powders from other suppliers (named GDC 2 and GDC 3) to attain a secured availability of commercial raw materials.

The components of the screen-printing pastes are the solvent terpineol, the binder ethyl cellulose and the corresponding GDC powder. The components are mixed in a defined ratio in a three-roll mill to form a homogeneously printable screen-printing paste. All the paste parameters and all the screen-printing settings were kept constant. The same counts for the sintering conditions of the GDC

Table I. Specific surface area and particle size distributions of the GDC powders.

ID	Powder supplier	BET surface [a] [m^2 g^{-1}]	Particle size distributions				Comments
			d10 [μm]	d50 [μm]	d90 [μm]	d50 [a] [μm]	
GDC 1	Treibacher Industrie AG	8.3	0.13	2.53	8.75	0.29	Strong agglomerates
GDC 2	Solvay	7.8	0.08	0.16	1.33	0.16	Soft agglomerates
GDC 3	KCeracell	6.74	0.12	0.67	4.69	0.22	Strong agglomerates

a) values given by the supplier

layer (1300 °C, 5 h). The main governing factor for hindering the Sr-YSZ interaction is not the gas tightness or the processing of the GDC but a well-formed interlayer between GDC and YSZ. The influence of such an interlayer on the cell performance and resistance is negligible.

The powder characteristics are summarized in Table I and SEM micrographs (equipment: Zeiss G450, Oberkochen, Germany) of the raw powders are presented in Fig. 1. The in-house measured particle size distributions are calculated with the Mie-theory, thereby, taking the refractive index of the GDC (2.2) into account (Retsch Technology—Horiba partica LA-950 V2, Haan, Germany).

From Table I and Fig. 1, the following powder characteristics can be concluded:

- GDC 1 and GDC 3 are composed of strong agglomerates as the ultrasonic treatment within the measurement equipment was not able to disintegrate the agglomerates.
- GDC 2 shows more loosely packed agglomerates as the d90 value is clearly smaller than the value of the other two powders.
- The specific surface area, measured after the BET theory is roughly similar for all three powders.
- The d50 values given by the suppliers fit for GDC 2 but differ for GDC 1 and GDC 3.
- The SEM micrographs of all three powders show clearly the sub-micron sized structure of the individual particles.

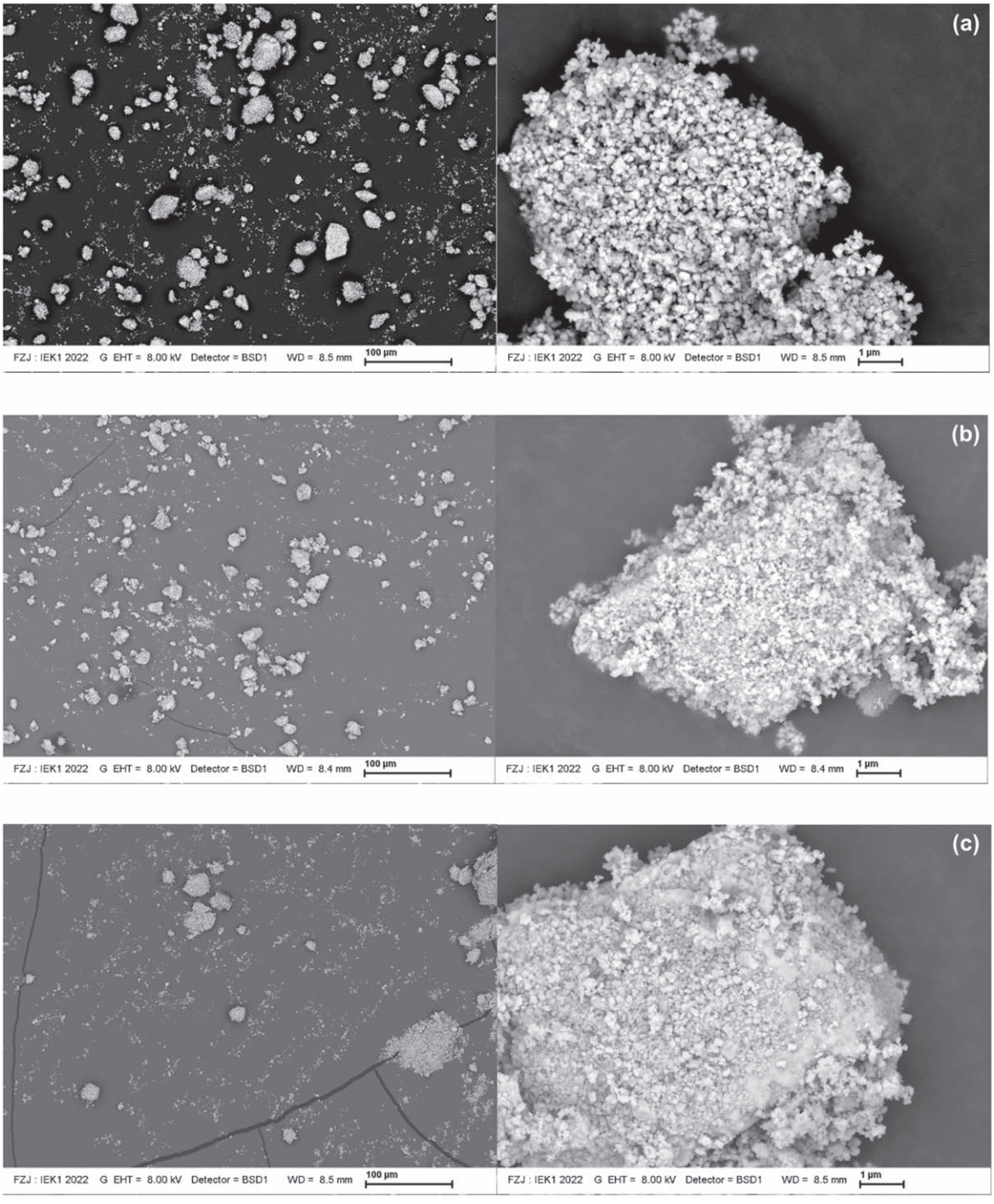

Figure 1. SEM micrographs of the GDC raw powders; (a) Treibacher Industrie AG—GDC 1 (b) Solvay—GDC 2 (c) KCeracell—GDC 3.

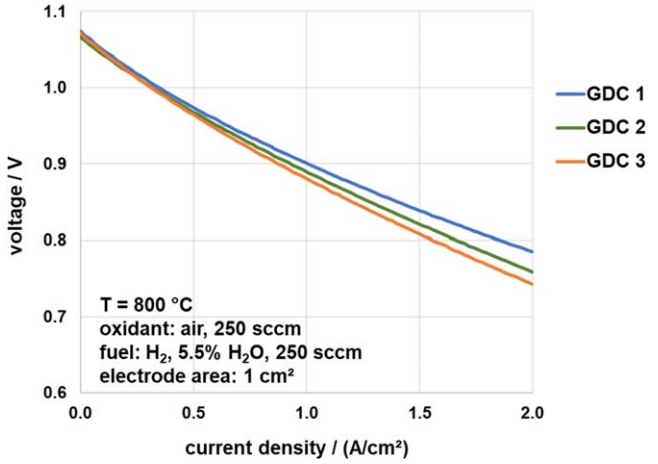

Figure 2. CV-characteristics of three full cells differing only with respect to the GDC powders applied for the GDC-interlayer between LSCF-cathode and 8YSZ-electrolyte. The cells were supplied with ambient air as the oxidant and humidified hydrogen (5.5% H_2O) at the fuel electrode.

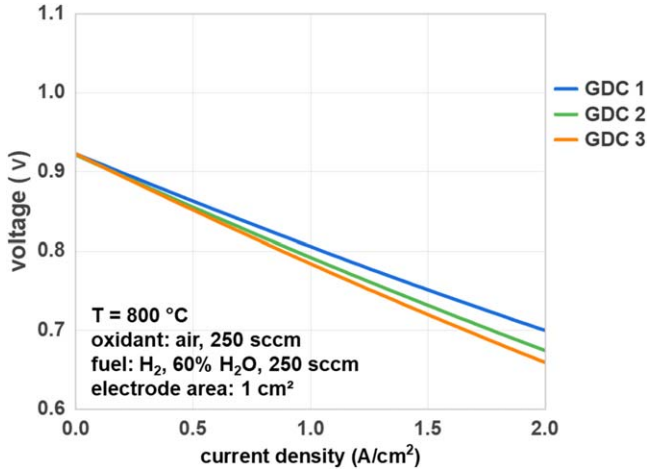

Figure 3. CV-characteristics of three full cells differing only with respect to the GDC powders applied for the GDC-interlayer between LSCF-cathode and 8YSZ-electrolyte. The cells were supplied with ambient air as the oxidant and humidified hydrogen (60% H_2O) at the fuel electrode.

- All particles show similar shapes, thus from an optical point of view it seems that an influence on the packing or sintering behavior does not exist.

Therefore, electrochemical characterization approaches and testing facilities were applied for the characterization of FESCs and symmetrical cells as described in Ref. 11. The cells exhibited an active electrode area of 1 cm^2 and a gas flow rate of 250 sccm per electrode was applied. Thus, the lateral gradients of temperature and the current density as well as the gas conversion can be neglected. During the testing phase, the operating conditions were varied systematically. Individual fuel and oxidant gas mixtures can be set via a gas mixing unit with Mass Flow Controllers (MFCs). These tests were performed with ambient air as the oxidant and hydrogen (H_2) as the fuel.

The performance of the cells was assessed by Current-Voltage (CV) characteristics (FESCs only) and EIS (FESCs and SymAEs) at OCV conditions. Next to an operando impedance measurement at nominal operating temperatures (850 °C–600 °C), additional low temperature impedance measurements between 600 °C and 250 °C were performed to obtain additional information about charge transport processes in the electrolyte. The spectra for higher temperatures were measured in galvanostatic mode (voltage amplitude ⩽12 mV) as described in Ref. 11, whereas the potentiostatic mode was chosen below 600 °C. As the electrolyte processes are linear, a higher amplitude of 200 mV was chosen. Reference measurements at the beginning and end of each cell tests were conducted in order to exclude aging effects. The validity of the measured spectra was verified by a Kramers Kronig test.[12] For further analysis the spectra were deconvoluted by the Distribution of Relaxation Times (DRT).

After testing, SEM analysis of the symmetrical cells was performed with a Thermo Scientific™ Helios G4 FX DualBeam™ (Thermo Fisher Scientific, Waltham, Massachusetts, USA) microscope to study the microstructural differences. Material contrast was obtained by backscattered-electron imaging using the in-column backscattered-electron detectors (Mirror Detector (MD) and In-Column detector (ICD)). Imaging was performed at electron energies between 3 and 5 keV.

Results and Discussion

The performance of the three FESCs differing only with respect to their GDC-interlayer was evaluated by means of CV characteristics and EIS. Three cells for each GDC (from a single supplier) were characterized using the same protocol to determine the reproducibility of the study. Additionally, the reference measurements were conducted to study the deviations and to eliminate the possibility of expected variations during testing. The resulting standard deviation of the cells in the cell performance was close to zero (0.0008), which omitted the possibility of having the differences due to measurements.

The fuel gas composition is composed of a mixture of hydrogen and steam to avoid oxidation of nickel in the fuel electrode. The OCV reaches 1.073 V at 800 °C for the cell operating with 5.5% humidity, just slightly lower than the theoretical value (∼1.08 V). Differences in the overall cell performance with a lower steam content (fuel with 5.5% humidity) can be clearly seen in Fig. 2. At a cell voltage of 0.8 V current densities of 1.86 A cm^{-2} (GDC 1), 1.67 A cm^{-2} (GDC 2) and 1.56 A cm^{-2} (GDC 3) were achieved at 800 °C.

As minor differences were observed between different GDCs, analysis is repeated for another gas composition (fuel with 60% humidity), resulting in the performance of the cells in the same order as shown in Fig. 3.

To attain a better understanding of the impact of different GDC powders, impedance spectra for three different cell types were compared at 800 °C. Figure 4 shows the spectrum of full cells with LSCF air electrode and Ni/YSZ fuel electrode with 5.5% and 60% steam.

The presence of higher steam content significantly reduces the low-frequency impedance and the lower frequency contribution of the electrode response is the most affected as shown in Fig. 4. The improvement of polarization resistance with higher humidity in hydrogen is also coherent with the investigations done in a previous study.[13] Based on this observation, it could be suspected that this contribution is associated with a gas diffusional process in the porosities of the electrode.

Moreover, it can be also seen that the spectra are similar at 800 °C, therefore, the impact of GDC powders cannot be studied at such higher temperatures. Nevertheless, since the ohmic resistance includes the resistance of the GDC interlayer while keeping the electrolyte and contact resistance constant, differences in the initial ohmic resistance are expected. These differences due to the GDC interlayer and the interfaces connected are clearly visible in Table II, in increasing order from GDC 1 to GDC 3.

In addition, to analyze the impact of GDC powders a thorough analysis of these differences based on EIS and DRT was done to evaluate the processes responsible for these performance differences. Impedance spectra were measured at OCV over a broad range of temperatures ranging from 850 °C to 250 °C with steps of 50 °C. In

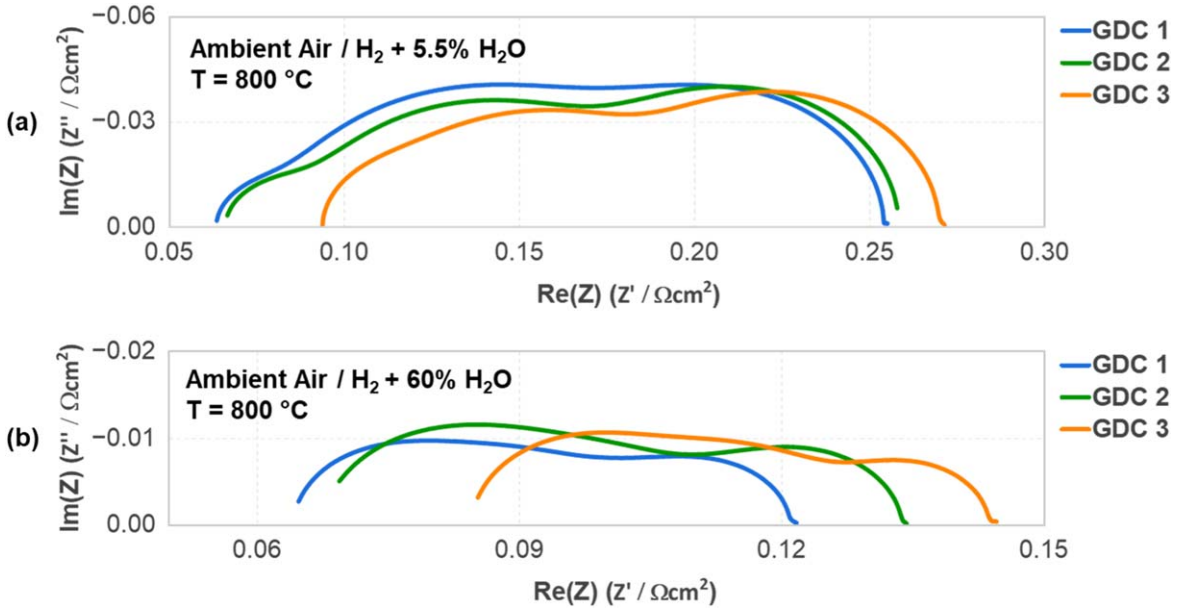

Figure 4. Impedance spectra of FESCs for three different types of cells with different GDC powders at temperature 800 °C measured with a fuel gas composition of humidified H_2 (a) with 5.5% H_2O and (b) with 60% H_2O and ambient air as oxidant.

Table II. Ohmic and polarization resistances of FESCs for three different types of cells with different GDC powders at temperature 800 °C measured with a fuel gas composition of humidified H2 (5.5% H_2O and 60% H_2O) and ambient air as oxidant.

Resistance (Ωcm^2)	60% H_2O (humidified H_2)		
	GDC 1	GDC 2	GDC 3
Ohmic	0.057	0.068	0.085
Polarization	0.064	0.065	0.60

The processes at the air electrode (cathode) and fuel electrode (anode) at higher temperatures are named according to Leonide et al.[7,15] P_{1A} represents gas diffusion within the Ni/YSZ anode substrate described by a generalized finite length Warburg element. As the gas diffusion resistance is not thermally activated and even decreases with decreasing temperature, this process is only dominant at high temperatures (850 °C–700 °C). P_{2A} and P_{3A} are related to the coupling of gas diffusion and ionic transport via the charge transfer reaction in the fuel electrode.[16] They are thermally activated and thus increase with decreasing operating temperature. Considering an exponential temperature dependency of the resistances but only minor changes in the capacitive behavior, the relaxation frequencies

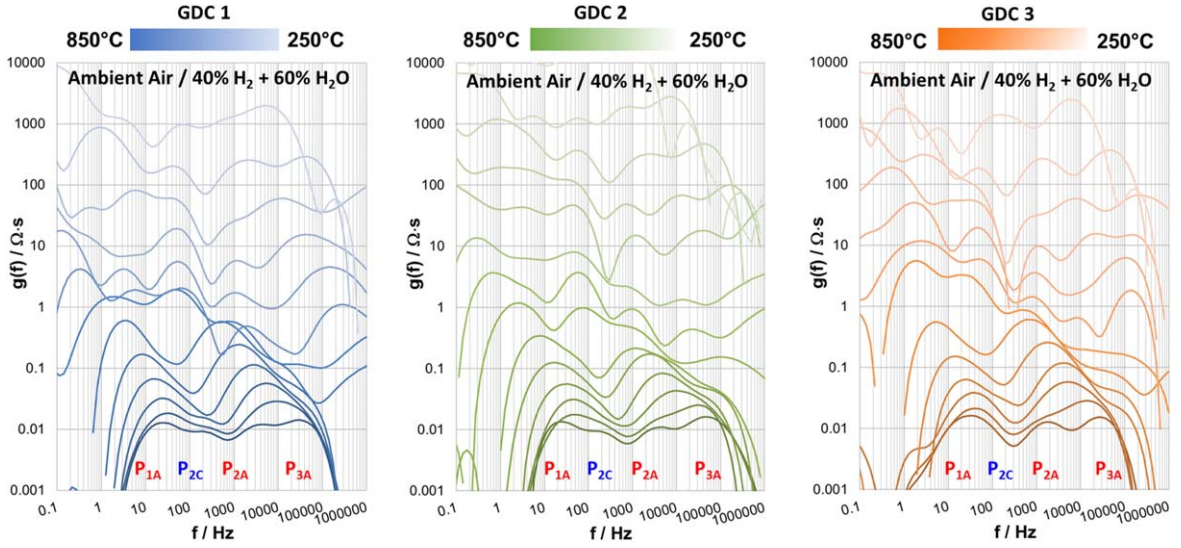

Figure 5. DRTs of impedance spectra of FESCs in a temperature range from 850 °C to 250 °C measured with a fuel gas composition of 60% H_2O and 40% H_2 and ambient air as oxidant.

Fig. 5 the DRTs of these spectra calculated by means of the method described in Ref. 14 are displayed. A logarithmic Y-scale is applied to visualize the DRTs over this wide temperature range, please consider that in these plots the geometrical area underneath a peak no longer corresponds to the related polarization resistance.

$f_r \propto 1/RC$ of these processes are shifted towards lower values.

P_{2C} accounts for the losses resulting from oxygen exchange at the LSCF-surface and oxygen ion transport in the LSCF bulk, described by a Gerischer element. As oxygen exchange and ionic transport are strongly thermally activated,[7] the peak increases and shifts towards

lower frequencies if the operating temperature is decreased. It should be noted that P_{1A} and P_{2C} are both of Transmission Line Model (TLM) type, exhibiting several peaks in the DRT,[17] which strongly overlap. At higher temperatures, the second peak of the Warburg element covers the rather small main peak of the air electrode, at lower temperatures the main peak of the Gerischer element is significantly increased and covers $P_{1A.}$ Furthermore, all other processes in the frequency range from several 100 Hz to several 100 kHz are covered by the dominating processes P_{2A} and P_{3A} of the fuel electrode.

In an impedance spectrum, the separation of ohmic and polarization resistance is straightforward. Commonly the ohmic resistance is attributed to the electrolyte, whereas the polarization resistance includes the different losses in the electrodes as gas diffusion and charge transfer related polarization phenomena.[7,14,15] Next to the electrodes, the highly resistive interphases (as well as interfaces) between ionic conducting phases, i.e. GDC and 8YSZ, can show a dielectric polarization and thus contribute to the polarization resistance. An interphase with a conductivity σ_i and a permittivity ε_i will show a relaxation type behavior with a relaxation frequency $f_i = \sigma_i/(2\pi\varepsilon_i)$. Often the conductivity of such interphases is still rather high (10^{-6} to 10^{-4} S cm^{-1}),[8] resulting in high relaxation frequencies in the range from several 10 kHz to >10 MHz. Processes with lower relaxation frequencies will overlap with electrochemical processes in the kHz range, namely P_{2A} and P_{3A} of the Ni/YSZ fuel electrode, whereas those in the MHz-range can hardly be measured accurately at higher temperatures. At temperatures below 600 °C further high frequency processes related to grain boundary and bulk contributions of the electrolyte layers occur in the DRTs. A reliable separation of these contributions is impeded by the overlapping of higher order peaks resulting from the TLM behavior[17] of the fuel electrode. Therefore, those in the MHz-range can hardly be measured accurately at higher temperatures.

To analyze the processes related to GDC-interlayer and secondary SZO-phases formed between GDC and YSZ, symmetrical cells without polarization phenomena at the fuel electrode (P_{1A}, P_{2A} and P_{3A}) combined with additional measurements below the nominal operating temperature are preferential. This becomes obvious from the DRTs of such cells displayed in Fig. 5 and Fig. 6.

Through the comparison of full cell, symmetrical air electrode and GDC palette, it can be seen that the formation of SZO is completely overshadowed by the fuel electrode peaks (P_{2A} and P_{3A}). Additionally, P_{SZO} vanishes almost entirely for a symmetrical air electrode cell exhibiting a GDC instead of a YSZ substrate as shown in Fig. 6.

By the application of symmetrical cells, which removes fuel electrode processes, four processes can be resolved in the DRT as shown in Fig. 7. These are related to gas diffusion (P_{1C}), oxygen surface exchange and diffusion in LSCF (P_{2C}), the charge transfer at the LSCF/GDC interface (P_{CT}) and, in case of a zirconia-based electrolyte, a 4th process P_{SZO} attributed to the GDC/YSZ-interface and the SZO-interphase formed there during sintering of the air electrode. The enlarged gas diffusion peak P_{1C} is related to differences in gas flow configuration.[18] It should be noted that the formation of an SZO-interphase consumes strontium from the LSCF-cathode and thus affects the composition of the LSCF, which can alter the related impedance contributions (P_{2C}, P_{CT}).

After eliminating the anode processes, the EIS measurements of SymAE show an enlarged air electrode gas diffusion. This is mainly related to gas flow configuration. In Fig. 7 the DRTs of three symmetrical cells differing only with respect to their GDC layers are shown for the temperature range from 850 °C to 250 °C. P_{2C}, P_{CT} and P_{SZO} exhibit a strong temperature dependency, their relaxation frequency shifts toward lower values with decreasing operating temperature. This is to be expected as the resistivity shows an exponential temperature dependency whereas the related capacity is commonly less temperature dependent.

In Fig. 8 the processes related to the LSCF/GDC/YSZ interface are displayed for a temperature range from 600 °C to 450 °C. This temperature range reveals the peak for the SZO interphase in a frequency range of 100 Hz to 1 kHz enabling highly accurate DRTs.

Additionally, a systematic comparison of three different commercially available GDC powders is presented based on the losses. The ohmic resistance was determined and it increased from GDC 1 to GDC 3 following the same order as discussed for full cells. This phenomenon is consistent at different testing temperatures as shown in Fig. 9.

To further analyze the differences with respect to the GDC interlayer, the comparison of polarization losses was done. Figure 10 shows the DRT spectra of the cells with the different GDC-interlayers. The cell performance values from CV characteristics (Fig. 2 and Fig. 3) are in good agreement with P_{SZO} in the DRT. The GDC 1 full cell showed the best performance and by far the lowest P_{SZO} in the DRT; in case of GDC 2 and GDC 3 much larger P_{SZO}-peaks can be observed, which are qualitatively in agreement with the cell performance values of the full cells. It should be noted

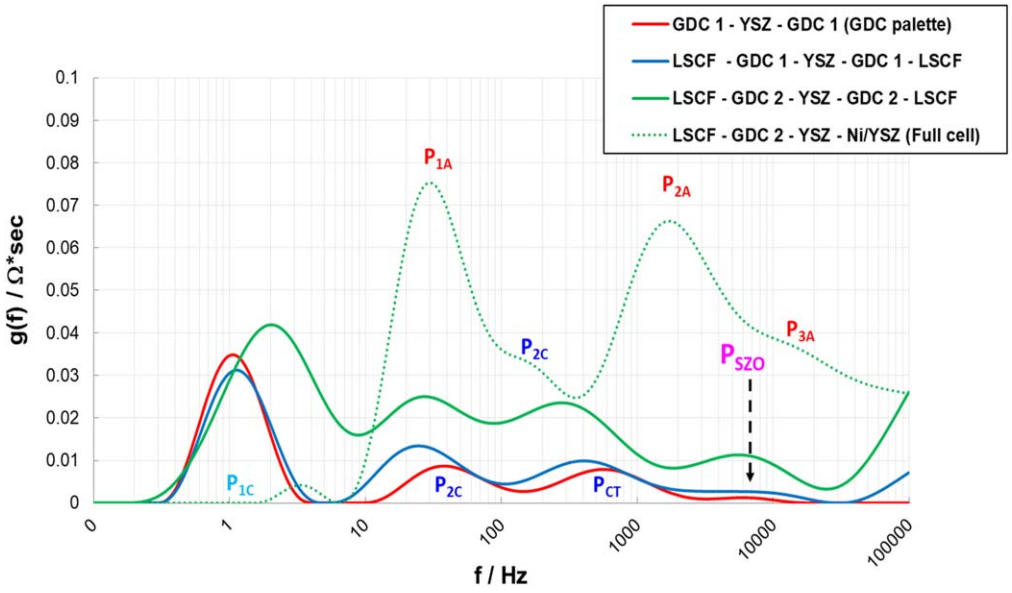

Figure 6. Comparison of DRTs measured with ambient air as oxidant to identify SZO formation in different GDC layers with and without electrolyte substrates at 750 °C.

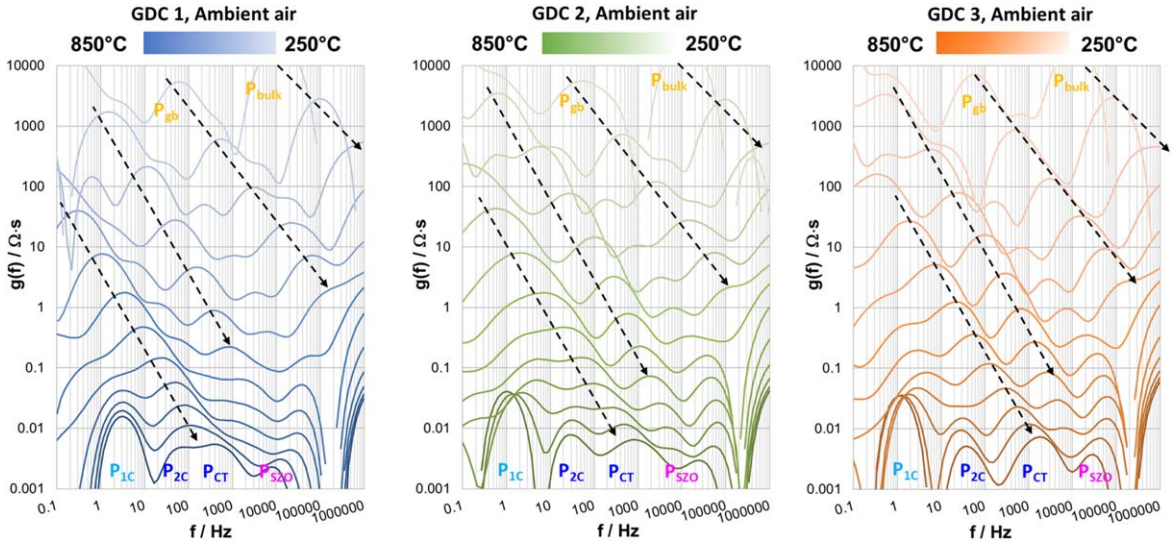

Figure 7. DRTs of impedance spectra of SymAE cells measured in a temperature range from 850 °C to 250 °C with ambient air as oxidant. The DRTs represent the air electrode polarization including contributions from GDC-interlayer and interphases at the GDC/8YSZ-interface. At lower temperatures further contributions related to grain boundary and bulk of the electrolyte substrate appear at higher frequencies.

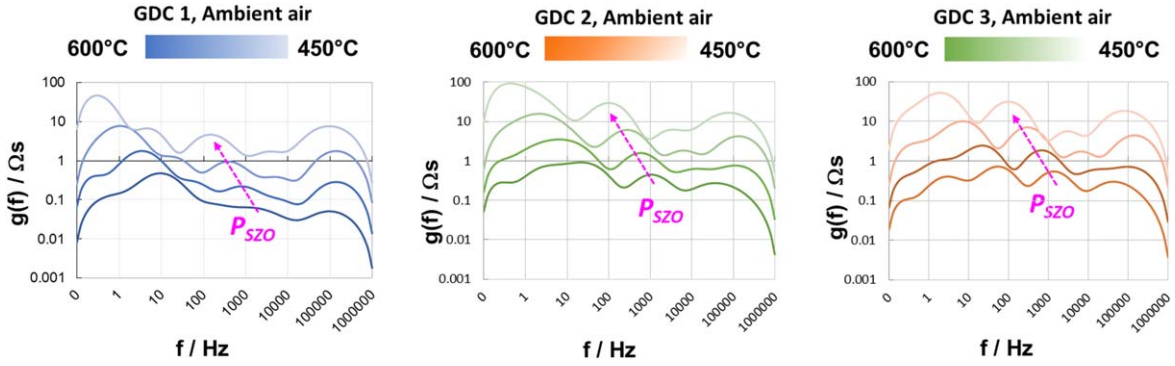

Figure 8. DRTs focusing on charge transfer and zirconate formation contributions from GDC-interlayer and interphases at the GDC/8YSZ-interface.

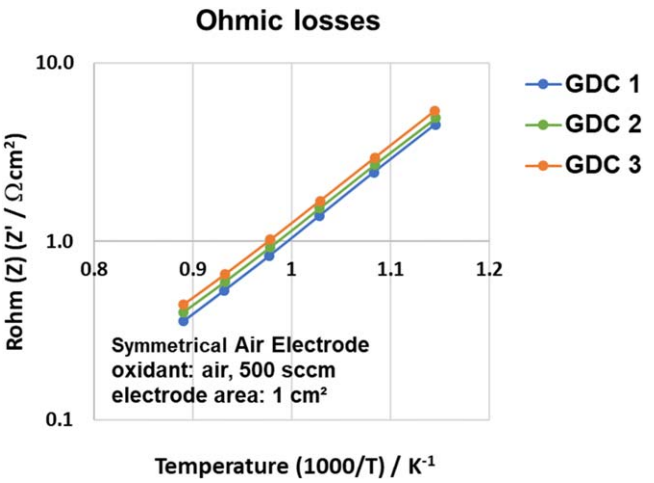

Figure 9. Comparison of ohmic losses in a temperature range from 850 °C to 600 °C with ambient air as oxidant for all the cells with three different GDC interlayers.

that not solely P_{SZO} differs between the three cells; there is also an impact on further polarization contributions of the air electrode and, in case of the full cells, minor variations in electrolyte and fuel electrode substrate.

Additionally, Fig. 11 reveals FIB-polished cross sections of the 3 GDC layers. The samples were prepared and analyzed according to the method described in Ref. 8. Based on the different greyscales the images enable us to distinguish between GDC, YSZ, the GDC/YSZ interdiffusion zone and SZO formed close to this interface. Whereas in the case of GDC 1 the SZO appearance is limited to small, restricted areas and a significant part of the interface exhibits direct contact between GDC and YSZ (via the Interdiffusion (ID) - zone), in the case of GDC 2 and GDC 3 a larger amount of SZO has been formed.

The boxes below the figures give evidence of the amount and continuity of the SZO-interphase. To obtain more precise information the area fraction of SZO in the boundary region was quantified. Even though these values do not correspond to the SZO volume fractions, they enable a quantitative comparison of the samples. In none of the samples, a continuous SZO-layer was formed. As shown in Ref. 2 this is essential for a functioning cell, a continuous SZO layer as observed for lowered GDC sintering temperatures results in a very high polarization resistance and low cell performance. Whereas large parts of the GDC 1 interface are free from SZO, GDC 2 and 3 clearly exhibit larger amounts of SZO, responsible for the lowering of the cell performance. The increased amount of SZO in these samples has to be attributed to the higher porosity of the GDC-interlayers. GDC 2 and 3 exhibit a higher porosity and larger thickness despite of similar powder preprocessing, screen printing paste preparation, screen printing and sintering. The observed differences most probably have to be attributed to different sintering

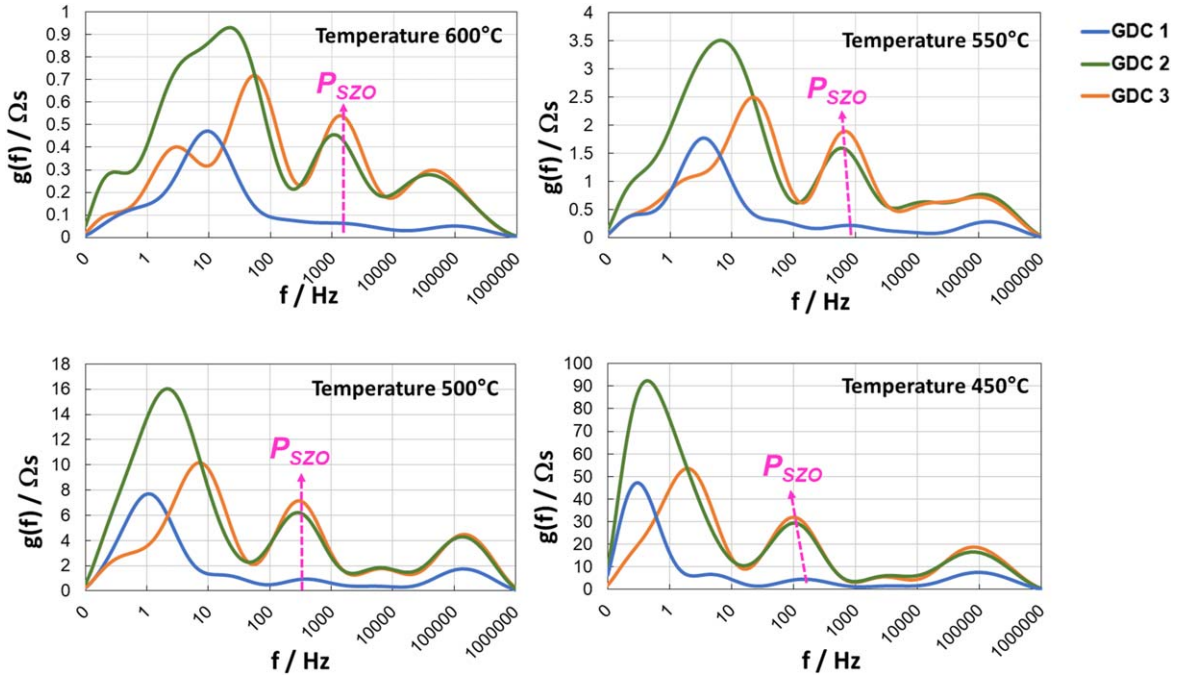

Figure 10. DRT comparison of cells in a temperature range from 600 °C to 450 °C with ambient air as oxidant with three different GDC interlayers.

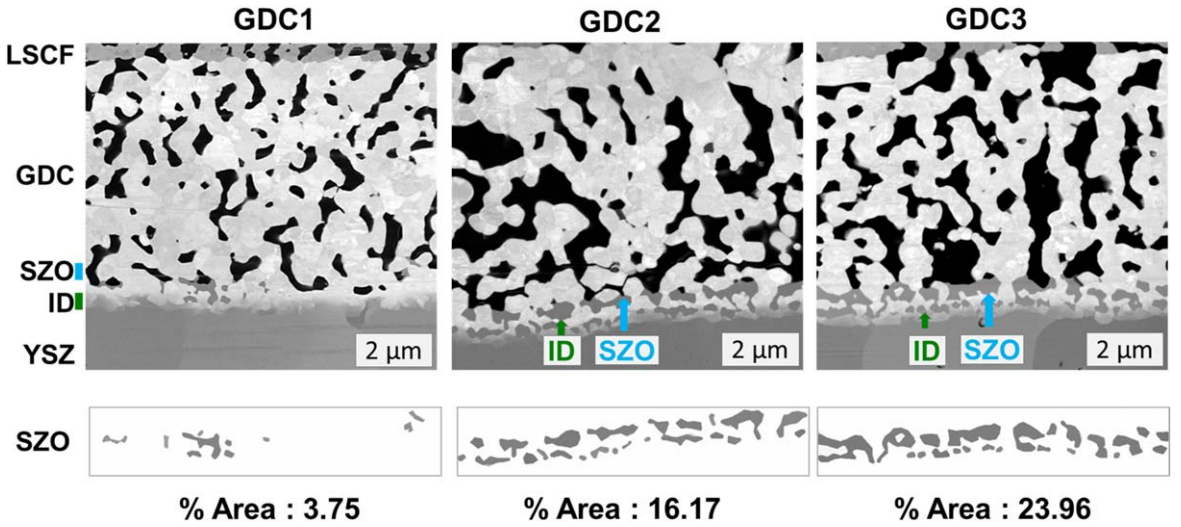

Figure 11. FIB-polished cross sections of the 3 GDC interlayers. The differences in porosity are obvious, GDC 2 and GDC 3 exhibit a higher porosity. Between the porous GDC interlayer and the dense YSZ electrolyte the interdiffusion zone (ID) and the non-continuous SZO-interphase (dark grey) and is visible. The lateral distribution of this SZO-interphase at the GDC/YSZ-interface is shown in the boxes below the picture. The SZO-amount differs significantly between the 3 samples.

kinetics of the three powders. Even though there are only small differences in the powder properties and the GDC 1 powder exhibits the largest particle sizes, the density and suppression of SZO-formation of the GDC 1 layer is the highest.

Intentionally all processing steps were kept constant to provoke microstructural differences and subsequently their impact on SZO formation and finally on performance. This highlights the high need for knowledge and tailoring of adequate powder pre-history, paste formulation, screen printer settings and drying/sintering regime to ensure high layer and cell quality.

Conclusions

The availability of raw materials from different suppliers and their suitability for established SOC production processes is essential for the commercialization of SOC. In this study, three GDC-powders from different suppliers were evaluated with respect to their applicability for GDC-interlayers in high performance fuel-electrode supported solid oxide cells. To enable a comparison of the powders similar powder preprocessing, screen printing paste preparation, screen printing and sintering procedures were applied.

The cells have been evaluated by means of current-voltage characteristics and impedance spectroscopy. Impedance analysis was carried out over a wide range of temperatures from 850 °C to 250 °C. The DRT analysis of full cells turned out to be challenging as the impedance contribution of the fuel electrode overlaps with processes at the air electrode/electrolyte interface. To eliminate the fuel electrode contribution, symmetrical air electrode cells were applied. DRT analysis of these cells revealed a clearer picture. Loss contributions related to a different extent of an SZO-interphase

formed during air electrode sintering could be resolved in the DRT. The electrochemical results obtained from CV characteristics and impedance spectra were confirmed with microstructural analysis revealing different amounts of SZO formed at the GDC/YSZ-interface. Despite a similar composition and identical preparation, the GDC - interlayers revealed clear differences. GDC - layers exhibiting a higher porosity showed larger amounts of SZO at their interface to the YSZ-electrolyte after air electrode sintering, which resulted in a considerable decrease in cell performance.

Acknowledgments

The authors gratefully acknowledge funding from the German Federal Ministry of Education and Research via the project "SOC Degradation 2.0" (BMBF 03SF0621G+A).

ORCID

Sadhana Golani https://orcid.org/0000-0003-3715-1390
Norbert H. Menzler https://orcid.org/0000-0001-7091-0980
André Weber https://orcid.org/0000-0003-1744-3732

References

1. V. Wilde, H. Störmer, J. Szász, F. Wankmüller, E. Ivers-Tiffee, and D. Gerthsen, *ACS Appl. Energy Mater.*, **1**, 6790 (2018).
2. J. Szász, F. Wankmüller, V. Wilde, H. Störmer, D. Gerthsen, N. H. Menzler, and E. Ivers-Tiffée, *J. Electrochem. Soc.*, **165**, F898 (2018).
3. A. Tsoga, A. Naoumidis, A. Gupta, and D. Stöver, *Mater. Sci. Forum*, **308–311**, 794 (1999).
4. J. T. Chou, Y. Inoue, T. Kawabata, J. Matsuda, S. Taniguchi, and K. Sasaki, *J. Electrochem. Soc.*, **165**, F959 (2019).
5. A. Tsoga, A. Gupta, A. Naoumidisa, and P. Nikolopoulos, *Elsevier*, **48**, 4709 (2000).
6. S. Uhlenbruck, N. Jordan, D. Sebold, H. P. Buchkremer, V. A. C. Haanappel, and D. Stöver, *Thin Solid Films*, **515**, 4053 (2007).
7. A. Leonide, S. Hansmann, A. Weber, and E. Ivers-Tiffée, *J. Power Sources*, **196**, 7343 (2011).
8. F. Wankmüller, J. Szász, J. Joos, V. Wilde, H. Stormer, D. Gerthsen, and E. Ivers-Tiffee, *J. Power Sources*, **360**, 399 (2017).
9. R. Steinberger-Wilckens, L. Blum, H. P. Buchkremer, L. G. J. De Haart, M. Pap, R. W. Steinbrech, S. Uhlenbruck, and F. Tietz, *Solid Oxide Fuel Cells 11*, **25**, 213 (2009).
10. A. Mai, V. A. C. Haanappel, F. Tietz, and D. Stöver, *Solid State Ionics*, **177**, 19 (2006).
11. D. Klotz, A. Weber, and E. Ivers-Tiffée, *Electrochim. Acta*, **227**, 110 (2017).
12. M. Schönleber, D. Klotz, and E. Ivers-Tiffée, *Electrochim. Acta*, **131**, 20 (2014).
13. F. Monaco, E. Effori, M. Hubert, E. Siebert, G. Geneste, B. Morel, E. Djurado, D. Montinaro, and J. Laurencin, *Electrochim. Acta*, **389**, 20 (2021).
14. A. Leonide, V. Sonn, A. Weber, and E. Ivers-Tiffée, *J. Electrochem. Soc.*, **155**, B36 (2007).
15. V. Sonn, A. Leonide, and E. Ivers-Tiffée, *J. Electrochem. Soc.*, **155**, B675 (2008).
16. S. Dierickx, T. Mundloch, A. Weber, and E. Ivers-Tiffée, *J. Power Sources*, **415**, 69 (2019).
17. A. Weber, *Tech. Mess.*, **88**, 1 (2021).
18. N. H. Menzler, J. Malzbender, P. Schoderböck, R. Kauert, and H. P. Buchkremer, *Fuel Cells*, **14**, 96 (2014).